Simultaneous Identification of Multiple Mechanical Parameters in a Servo Drive System Using Only One Speed

Yuefei Zuo, *Member, IEEE*, Jie Mei, *Student Member, IEEE*, Xinan Zhang, *Member, IEEE*, and Christopher H. T. Lee, *Senior Member, IEEE*

***Abstract* –In some servo applications, restricted by the measurement noise and the stiffness of the mechanical system, the bandwidth of the disturbance observer cannot be high enough to realize a good robust control to parameters uncertainties, it is essential to identify the mechanical parameters. In the existing mechanical parameter identification methods, the viscous and Coulomb friction torque coefficients are usually identified using two different constant speeds, and the moment of inertia can be identified with various methods. However, no one method can identify these three parameters at the same time using only one speed. The contribution of this paper is to propose a method that can identify the three mechanical parameters simultaneously using only one speed. A low pass filter is used to suppress the measurement noise in the speed feedback, thus parameters are identified with high precision. A unidirectional sine-wave speed is used to decouple the viscous friction torque and the Coulomb friction torque, two speeds with different amplitudes and the detection of the speed amplitude are no more required. Adaptive extended state observer (ESO) is designed based on Lyapunov's stability theory, can be easily changed to the normal ESO used in active disturbance rejection control. The proposed method is easy to understand and implement. The effectiveness of the method is verified by both the simulation and experimental results. [1]**

Index Terms - Active disturbance rejection control, adaptive extended state observer, Coulomb friction torque, inertia identification, viscous friction torque coefficient.

I. INTRODUCTION

DUE to its advantageous features including high efficiency, high-power density, large torque-to-inertia ratio, low noise, and free maintenance [1], permanent magnet synchronous motor (PMSM) has been widely used in servo applications. Nevertheless, the mechanical dynamics of electrical drives are nonlinear and usually time-varying. Traditional one-degree-of-freedom (1DOF) proportional-integral (PI) controller cannot be used to obtain both good speed-reference tracking and excellent load-torque rejection. The alternative is to employ two-degree-of-freedom (2DOF) robust control methods [2], in which disturbance/uncertainty estimation and attenuation (DUEA) techniques are widely used [3]. Among many DUEA techniques, disturbance observer (DOB) and extended state observer (ESO) are most extensively investigated and applied. DOB was initiatively put forward by Ohnishi and his colleagues in 1980s to estimate the external disturbance of servo systems [4]. ESO is generally regarded as an essential part of the so-called active disturbance rejection control (ADRC), which was first proposed by Han [5].

Both DOB and ESO estimate the disturbance torque according to the equation of motion, in which the control gain, the ratio between torque constant and inertia, plays a significant role [6]. In general, due to changes in load, the inertia may vary over a wide range from its nominal value to multiples of the nominal inertia, especially in direct drive systems, which results in larger overshoot and longer settling time [7]-[8]. Though mismatched inertia is sometimes beneficial for the disturbance rejection property, it has adverse effects on the tracking performance of continuously varying reference [9]. Except for the moment of inertia, other mechanical parameters (such as the coefficients of viscous friction torque and the Coulomb friction torque) are also essential to improve the position and speed control performance in the servo drive system. If the viscous and Coulomb friction torque coefficients are mismatched, the friction torque will be part of the total disturbance torque. Though the Coulomb friction torque is small, it changes very quickly when the motor changes direction, while the viscous friction torque varies as rapidly as the speed. To reject such fast time-varying disturbances, the bandwidth of the observer must be increased. However, the bandwidth of the observer is restricted by the measurement noise and the stiffness of the mechanical system.

Another approach to overcome parameter uncertainties is to identify them. Over the past three decades, many methods of identifying mechanical parameters have been developed. Normally, the viscous and Coulomb friction torque coefficients can be easily calculated from two different constant speeds [10]-[12], [13], [14] or three different constant speeds [15], depends on whether the constant load torque is zero. After that, the inertia can be calculated by using a constant accelerator

Manuscript received September 26, 2019; revised February 9, 2020; accepted June 1, 2020. This work was supported in part by the Start-Up Grant from Nanyang Technological University under Grant 04INS000574C140, and in part by the Natural Science Foundation of China under Grant 51807080. Recommended for publication by Associate Editor S. Lindsay. *(Corresponding author: Christopher H. T. Lee.)*

Y. Zuo is with the School of Electrical and Information Engineering, Jiangsu University, Zhenjiang 212013, China (e-mail: zuoyuefei@ujs.edu.cn)

J. Mei is with the Research Laboratory of Electronics, Massachusetts Institute of Technology, Cambridge, MA 02139, USA (e-mail: jiemei@mit.edu)

X. Zhang is with the School of Electrical, Electronic and Computer Engineering, University of Western Australia, Perth, WA 6009, Australia (e-mail: xinan.zhang@uwa.edu.au)

C. H. T. Lee is with the School of Electrical and Electronic Engineering, Nanyang Technological University, Singapore 639798, Singapore (e-mail: chtlee@ntu.edu.sg).

Color versions of one or more of the figures in this paper are available online at http://ieeexplore.ieee.org.

Digital Object Identifier

method [10]-[12], an offline curve fitting method [16], or the speed frequency response method [14]-[15]. In [17], the influence of viscous friction coefficient on inertia identification is eliminated by using the torque and acceleration information when the sinusoidal speed is zero. These types of direct calculation methods are fast, nevertheless, it is either noisy due to the use of velocity derivatives or time-consuming due to the detection of speed amplitude.

Another type of method adopts the adaptive state observer based on the equation of motion. Since the load torque is unknown, one kind of method is to eliminate it during the identification process. A simple way to eliminate constant load is differentiating motion equations, such as the recursive least square method [18] and the Landau model reference adaptive identification (MRAI) method [19]. However, since the viscous friction coefficient is ignored, the identified inertia is pulsating [20]. In order to eliminate the effect of load torque and viscous friction torque at the same time, a method integrating the product of estimated load torque and the accelerator based on the orthogonal principle was proposed by I. Awaya [21]. This method has been widely studied due to its good identification results [7], [9], [21]-[25]. However, to get a stable identification result, the bandwidth of DOB must be low enough to suppress the noise amplified by the speed differential, whereas it deteriorates the system dynamic performance. Andoh [22] takes FFT to smooth the waveform of motor position so that the method can be used with infinitesimal motions, but it greatly increases the consumption of computing resources. In [23], Y. Chen proposed a variable-period identification method, which no longer requires the low pass filter (LPF) to distinguish the speed, but the computation of varying period is quite complicated. In [24], the viscous friction coefficient was also identified with the integral method. In the above identification methods based on the orthogonal principle, the Coulomb friction torque is not considered. S. Kim [25] used the integral method to identify not only the moment of inertia but also the viscous and Coulomb friction torque, simultaneously. Since the method is based on the principle that the sinusoidal speed is in phase with the friction torque and out of phase with the inertia torque, it requires a knowledge of the magnitude of the speed response, while the detection of the magnitude complicates the calculation. Meanwhile, to decouple the Coulomb friction torque and the viscous friction torque, sinusoidal speeds with different amplitudes are required.

The other kind of method is to use MRAI to identify the load torque and the inertia simultaneously. In [26], an adaptation mechanism for identifying the moment of inertia and the load torque is given based on Popov's hyperstability theory. Nevertheless, it has not been experimentally verified, and both the viscous friction torque and the Coulomb friction torque are ignored. Moreover, four parameters in the two PI controllers need to be adjusted for the identification, which complicates the parameter setting process. In [27], K. Liu identified the inertia and the viscous friction coefficient simultaneously, and simplified the parameter setting process by using two integral controllers. However, the identified viscous friction coefficient converges to the wrong value and the identified moment of inertia is pulsating. Meanwhile, the Coulomb friction torque and the LPF for speed feedback are not considered.

In this paper, a method is proposed to identify the three mechanical parameters (the moment of inertia, the viscous and the Coulomb friction torque coefficients) simultaneously using only one speed. A low pass filter is used to suppress the measurement noise in the speed feedback, thus parameters are identified with high precision. A unidirectional sine-wave speed is used to decouple the viscous friction torque and the Coulomb friction torque, two speeds with different amplitudes and the detection of the speed amplitude are no more required. Adaptive extended state observer (ESO) is designed based on Lyapunov's stability theory, can be easily changed to the normal ESO used for active disturbance rejection control system. The proposed method is easy to understand and implement. The remaining paper is organized as follows. In Section II, a discussion on modeling the mechanical dynamics is presented, and then the design of conventional ADRC controller is introduced. In Section III, the adaptive ESO and the speed control system are designed for the identification of mechanical parameters. Simulation and experimental results are presented and analyzed in Section IV. Finally, conclusions are drawn in Section V.

II. ADRC Controller Design

The motion equation of the PMSM system can be given as

$$\dot{\Omega} = \frac{-B\Omega + T_e - T_L - T_c \operatorname{sign}(\Omega)}{J} \tag{1}$$

where Ω is the angular velocity, B and T_c are the viscous and Coulomb friction torque coefficients respectively, J is the moment of inertia, T_L is the load torque, and T_e is the electromagnetic torque.

A. Feedback Control Law

The feedback control law is designed to obtain the proper control quantity, i.e., the torque reference, so that the speed reference tracking error can attenuate as desired. As a result, the motion equation should be modified as a function of the torque reference T_e^*

$$\begin{aligned}\dot{\Omega} &= \frac{-B\Omega + T_e^* - T_c \operatorname{sign}(\Omega) - [T_e^* - T_e + T_L]}{J} \\ &= -\frac{B}{J}\Omega + \frac{1}{J}T_e^* - \frac{T_c}{J}\operatorname{sign}(\Omega) - \frac{T_{d\_ex}}{J} \\ &= -a\Omega + bT_e^* - c\operatorname{sign}(\Omega) - d_{ex}\end{aligned} \tag{2}$$

where $T_{d\_ex}=T_e^*-T_e+T_L$ is the external disturbance torque which includes the electromagnetic torque tracking error and the load torque, $a=B/J$ is the state coefficient, $b=1/J$ is the control gain, $c=T_c/J$ is another state coefficient, and $d_{ex}=T_{d\_ex}/J$ is the total disturbance angular accelerator. Generally, due to the fast dynamics of the current control loop, the electromagnetic torque tracking error can be neglected, i.e., $T_e^* \approx T_e$.

Defining the reference of mechanical angular velocity as Ω^*, then the tracking error of mechanical angular velocity can be expressed as $e_s=\Omega^*-\Omega$ and we have

$$\dot{e}_s = \dot{\Omega}^* - \dot{\Omega} = \dot{\Omega}^* - bT_e^* + a\Omega + c\operatorname{sign}(\Omega) + d_{ex} \tag{3}$$

Combined (3) with linear feedback control law

$$\dot{e}_s = -k_{ps} e_s \tag{4}$$

where k_{ps} is the proportional gain, and we have

$$T_e^* = \frac{\dot{\Omega}^* + k_{ps}(\Omega^* - \Omega) + a\Omega + c\,\mathrm{sign}(\Omega) + d_{ex}}{b} \tag{5}$$

In (5), the state coefficient a and c, the control gain b and the disturbance d_{ex} are generally unknown and usually substituted by their estimated value. Considering the viscous friction torque and the Coulomb friction torque are small, the estimated valued of a and c are commonly set to zero for simplification, i.e., $\hat{a} = \hat{c} = 0$, When a, b and c in (2) are substituted by their estimated value 0, $\hat{b}$ and 0, it can yield

$$\begin{aligned} \dot{\Omega} &= -a\Omega + bT_e^* - c\,\mathrm{sign}(\Omega) - d_{ex} \\ &= \hat{b}T_e^* - d_{ex} - a\Omega - (\hat{b} - b)T_e^* - c\,\mathrm{sign}(\Omega) \\ &= \hat{b}T_e^* - d_{to} \end{aligned} \tag{6}$$

where the total disturbance d_{to}, consisting of both external load disturbance and internal disturbance caused by parameter uncertainties, can be expressed by

$$d_{to} = d_{ex} - a\Omega + (\hat{b} - b)T_e^* - c\,\mathrm{sign}(\Omega) \tag{7}$$

Similarly, when d_{to} is substituted by its estimated value $\hat{d}_{to}$, the control quantity of the system can be obtained as

$$T_e^* = \frac{\dot{\Omega}^* + k_{ps}(\Omega^* - \Omega) + \hat{d}_{to}}{\hat{b}} \tag{8}$$

Considering that the actual system cannot provide infinite control output, saturation limit is usually applied as follows.

$$T_{esat}^* = \begin{cases} T_{e\max}^* \,\mathrm{sgn}(T_e^*), & \left|T_e^*\right| > T_{e\max}^* \\ T_e^*, & \left|T_e^*\right| \le T_{e\max}^* \end{cases} \tag{9}$$

B. Conventional ESO

It should be noted that there is always measurement noise δ_n in the measured speed, hence the actual measured speed is $y=\Omega+\delta_n$. In order to estimate the total disturbance, ESO is constructed for the system expressed by (6) and can be written in the form of

$$\begin{cases} \tilde{\Omega} = \hat{\Omega} - \Omega - \delta_n \\ \dot{\hat{\Omega}} = \hat{b}T_e^* - \hat{d}_{to} - k_1\tilde{\Omega} \\ \dot{\hat{d}}_{to} = k_2\tilde{\Omega} \end{cases} \tag{10}$$

where $\hat{\Omega}$ is the estimated angular velocity, $\tilde{\Omega}$ is the observational error, k_1 and k_2 are the gains of the observer.

Combining (1) and (10), the estimated speed and the observational error can be given as

$$\hat{\Omega}(s) = \Omega(s) + \frac{k_1 s + k_2}{s^2 + k_1 s + k_2}\delta_n(s) + \frac{s}{s^2 + k_1 s + k_2}d_{to}(s) \tag{11}$$

$$\tilde{\Omega}(s) = \frac{s}{s^2 + k_1 s + k_2}d_{to}(s) - \frac{s^2}{s^2 + k_1 s + k_2}\delta_n(s) \tag{12}$$

Choosing the characteristic polynomial of the observer to be $s^2+2\omega_o s+\omega_o^2=0$, then the gain of observer can be obtained as

$$\begin{cases} k_1 = 2\omega_o \\ k_2 = \omega_o^2 \end{cases} \tag{13}$$

where ω_o is the undamped natural frequency of the observer.

From (11), we know that the estimated speed is equal to the instant speed if the total disturbance is constant instead of time varying. Moreover, the measurement noise is also suppressed in the estimated speed. As a result, ESO is also used as an instantaneous speed observer, i.e., the estimated speed is used instead of the measured one as the speed feedback. However, according to (7), the total disturbance may be fast time varying due to the mismatched parameters, e.g., the disturbance torque caused by the Coulomb friction coefficient changes very quickly when speed changes direction.

The larger the deviations between the parameters and their actual values are, the bigger the total disturbance becomes, and subsequently the worse the system dynamic performance is getting. The increase of ω_o is beneficial for improving the dynamics of the observer and thus reduce the effect of the total disturbance on speed, but it is restricted by the measurement noise and the stiffness of the system. Consequently, in order to improve the system dynamic performance, it is essential to estimate parameters a, b and c.

III. Proposed Adaptive ESO for Mechanical Parameters Identification

A. Decoupling of the Two Friction Torques

It should be noted that the viscous friction torque and the Coulomb friction torque are coupled, as in (14) below

$$T_e = J\dot{\Omega} + (B\left|\Omega\right| + T_c)\,\mathrm{sign}(\Omega) + T_L \tag{14}$$

When the speed is bidirectional, the Coulomb friction torque is also bidirectional, just like the viscous friction torque. When the speed is unidirectional and constant, the Coulomb friction torque and the viscous friction torque are also unidirectional and constant, similar with the constant load torque. The two torques are coupled because they are of the same frequency. As a result, in these two situations, the identification of the two friction coefficients is impossible by only one speed.

To solve the problem, unidirectional time-varying speed is adopted for parameter identification. With this speed, the Coulomb friction torque is equal to the constant load torque, while the viscous friction torque changes over time. Since they are of different frequencies, they can be separated. Meanwhile, (1) is simplified by transforming the Coulomb friction torque to a constant load torque

$$\dot{\Omega} = \frac{-B\Omega + T_e - T_{Lc}}{J} = -a\Omega + bT_e - d \tag{15}$$

where T_{Lc} is the effective load torque due to the Coulomb friction torque, and $d=T_{Lc}/J$ can be seen as constant when the speed is unidirectional with an assumption that the Coulomb friction is constant.

B. Design of the Adaptive ESO

The ESO constructed for the system expressed by (15) can be

written as

$$\begin{cases} \tilde{\Omega} = \hat{\Omega} - \Omega \\ \dot{\tilde{\Omega}} = -\hat{a}\Omega + \hat{b}T_e - \hat{d} - k_1\tilde{\Omega} \\ \dot{\tilde{d}} = k_2\tilde{\Omega} \end{cases} \tag{16}$$

where $\hat{d}$ is the estimated value of d.

Subtracting (1) from (16) yields

$$\dot{\tilde{\Omega}} = \dot{\hat{\Omega}} - \dot{\Omega} = -k_1\tilde{\Omega} - \tilde{d} - \tilde{a}\Omega + \tilde{b}T_e \tag{17}$$

$$\dot{\tilde{d}} = k_2\tilde{\Omega} \tag{18}$$

where $\tilde{a}$, $\tilde{b}$ and $\tilde{d}$ are the estimating errors of a, b and d, and can be expressed as

$$\begin{cases} \tilde{a} = \hat{a} - a \\ \tilde{b} = \hat{b} - b \\ \tilde{d} = \hat{d} - d \end{cases} \tag{19}$$

According to the techniques used in backstepping control theory [28]-[29], the Lyapunov positive definite function V_1 can be selected as

$$V_1 = \frac{1}{2}\tilde{\Omega}^2 + \frac{1}{2k_2}\tilde{d}^2 + \frac{1}{2k_a}\tilde{a}^2 + \frac{1}{2k_b}\tilde{b}^2 \tag{20}$$

where the coefficient k_a and k_b are positive real number.

The derivative of V_1 can be expressed as

$$\dot{V}_1 = -k_1\tilde{\Omega}^2 + \frac{\tilde{a}}{k_a}\left(\dot{\tilde{a}} - k_a\Omega\tilde{\Omega}\right) + \frac{\tilde{b}}{k_b}\left(\dot{\tilde{b}} + k_b T_e\tilde{\Omega}\right) \tag{21}$$

Obviously, the first term on the right side of (21) is negative, hence stability of the observer can be guaranteed by making the two other terms on the right hand to be zero

$$\begin{cases} \dot{\tilde{a}} - k_a\Omega\tilde{\Omega} = 0 \\ \dot{\tilde{b}} + k_b T_e\tilde{\Omega} = 0 \end{cases} \tag{22}$$

Suppose the coefficients a and b remain constant during the identification process, that is

$$\begin{cases} \dot{\hat{a}} = \dot{\tilde{a}} + \dot{a} = \dot{\tilde{a}} = k_a\Omega\tilde{\Omega} \\ \dot{\hat{b}} = \dot{\tilde{b}} + \dot{b} = \dot{\tilde{b}} = -k_b T_e\tilde{\Omega} \end{cases} \tag{23}$$

then the adaptive law for a, b and d can be obtained as

$$\begin{cases} \hat{a}(t) = k_a\int \Omega\tilde{\Omega}dt + \hat{a}(0) \\ \hat{b}(t) = -k_b\int T_e\tilde{\Omega}dt + \hat{b}(0) \\ \hat{d}(t) = k_2\int \tilde{\Omega}dt + \hat{d}(0) \end{cases} \tag{24}$$

where $\hat{a}(0)$, $\hat{b}(0)$ and $\hat{d}(0)$ are the initial values of the estimated parameters $\hat{a}$, $\hat{b}$ and $\hat{d}$. $\hat{a}(0)$ and $\hat{d}(0)$ are usually set to zero.

Consequently, the estimated inertia, the viscous friction torque coefficient, and the total disturbance torque can be calculated as

$$\begin{cases} \hat{J}(t) = \dfrac{1}{\hat{b}(t)} = \dfrac{1}{-k_b\int T_e\tilde{\Omega}dt + \hat{b}(0)} \\ \hat{B}(t) = \dfrac{\hat{a}(t)}{\hat{b}(t)} = \hat{J}(t)\left[k_a\int \Omega\tilde{\Omega}dt + \hat{a}(0)\right] \\ \hat{T}_L(t) = \dfrac{\hat{d}(t)}{\hat{b}(t)} = \hat{J}(t)\left[k_2\int \tilde{\Omega}dt + \hat{d}(0)\right] \end{cases} \tag{25}$$

As shown in (25), T_e, $\tilde{\Omega}$ and Ω are used for the identification. A rapid change of them leads to a rapid change of the identified parameters. For more stable results, it is better to use a sinusoidal speed reference.

C. Suppression of the Measurement Noise in Speed Feedback

It can be known from (12) that the measurement noise is passed to the observational error through a high pass filter (HPF). Due to the integral operation, the estimated moment of inertia and the estimated disturbance torque are hardly affected by the measurement noise, while the estimated viscous friction torque coefficient is seriously affected. Smaller k_a and k_b are beneficial for suppressing the noise, whereas lead to longer identification time. Therefore, low bandwidth is adopted for the observer, and LPF is used for the speed feedback.

Assuming a first order LPF with a time constant of τ is used, then the relationship between the filtered speed Ω_f and the actual speed Ω can be expressed as

$$\Omega = \tau\dot{\Omega}_f + \Omega_f \tag{26}$$

Substituting (26) into (1) yields

$$(J + B\tau)\dot{\Omega}_f = -B\Omega_f - J\tau\ddot{\Omega}_f + T_e - T_{Lc} \tag{27}$$

Suppose a offset sinusoidal speed with an angular frequency of ω is adopted, and it can be expressed by $\Omega_f=\Omega_{fs}+\Omega_{fo}$, where Ω_{fs} and Ω_{fo} are the AC and DC component of the speed, respectively, then (27) becomes

$$\begin{aligned} J_1\dot{\Omega}_{fs} &= -(B - J\tau\omega^2)\Omega_{fs} + T_e - T_{Lc} \\ &= -B_1\Omega_{fs} + T_e - (T_{Lc} + B_1\Omega_{fo}) \end{aligned} \tag{28}$$

where $J_1=J+B\tau$ is the effective inertia and $B_1=B-J\tau\omega^2$ is the effective viscous friction coefficient.

It should be noted that the identified inertia is slightly deviates from its actual value since $B\tau$ is usually much smaller than J. However, the identified viscous friction torque coefficient may differ greatly from its actual value as the deviation $-J\tau\omega^2$ is proportional to ω^2. If B is not identified, the disturbance will be the sum of the load torque and the effective viscous friction torque, which varies with the speed. Since the disturbance is time-varying, a pulsating steady-state observational error will be generated, leading to a pulsating identified inertia.

To reduce the time varying disturbance torque, the same LPF is used for both the feedback speed and the torque in the proposed method. Assuming the filtered torque is T_{ef}, there is

$$\begin{aligned} J\dot{\Omega}_f &= -B\Omega_f + T_{ef} - T_{Lc} \\ &= -B\Omega_{fs} + T_{ef} - (T_{Lc} + B\Omega_{fo}) \end{aligned} \tag{29}$$

Since there is no time-varying disturbance torque in the

system expressed by (29), accurate J and B can be identified.

D. Control System for Parameter Identification

The block diagram of the speed control system for parameter identification is shown in Fig. 1, where the CL represents the current loop. In the parameter identification process, the two dotted lines are not connected, which means that the estimated disturbance is not feedforward for the disturbance compensation, and the control gain is calculated by the initial inertia instead of the identified one. In this case, the speed control performance is not affected by the identification. Using only a proportional gain to control the tracking error, it is easy to stabilize the system despite the steady-state tracking error. To reduce the tracking error, a larger proportional gain or initial inertia can be used.

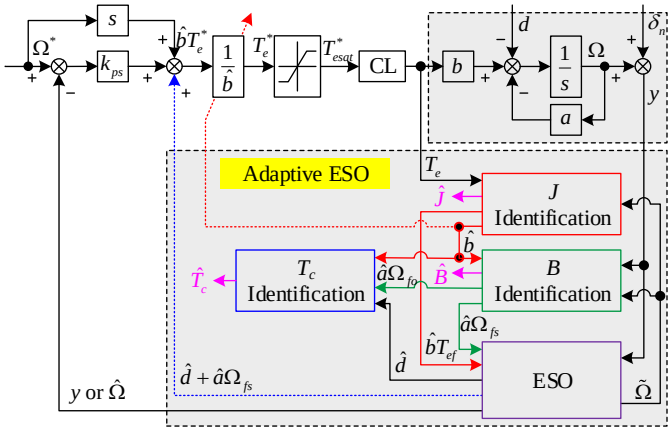

Fig. 1. ADRC controller for parameters identification.

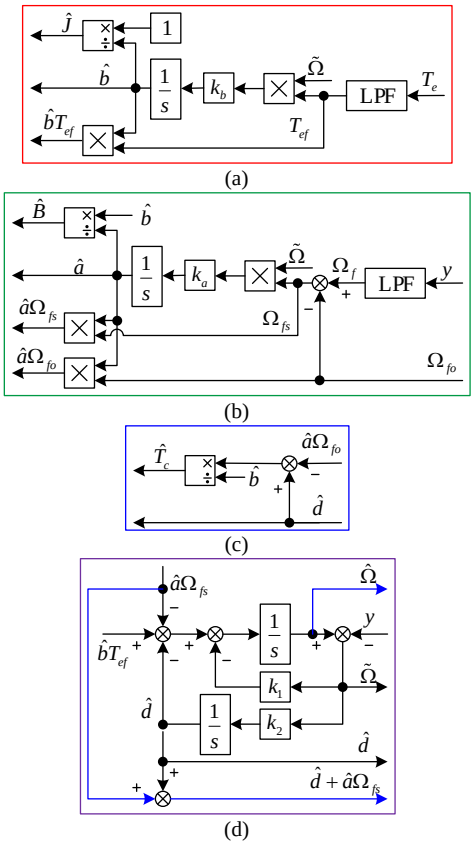

Fig. 2. Block diagram of the four modules. (a) Inertia Identification. (b) The viscous friction torque coefficient Identification. (c) The Coulomb friction torque coefficient Identification. (d) ESO.

After the mechanical parameters are identified, the control gain is updated by the identified inertia. Meanwhile, by disabling the identification modules and enabling the disturbance feedforward, the control system will be transformed into a normal ESO used in ADRC system. The identification modules can be disabled by simply setting k_a and k_b to zero. Fig. 2 shows the block diagram of the identification modules and ESO.

IV. Simulation and Experimental Results

In order to verify the proposed algorithm, MATLAB/Simulink simulation and experiment results are presented and analyzed in this section. The specification of the servo motor is shown in Table I.

As shown in Fig. 3, the control strategy is based on space vector pulse width modulation (SVPWM) control with i_d^*=0. Decoupled PI regulators are employed in the current-loop to control i_d and i_q respectively, and adaptive ADRC controller is employed in the speed-loop. The DC bus voltage u_{dc} is 150V. The saturation limit of q-axis reference current is 9 A. The bandwidths of d-axis and q-axis current-loops are 2000 rad/s. The feedback control gain k_{ps} is set to 100, the natural frequency of ESO is set to 50 rad/s, i.e., k_1 and k_2 are 100 and 2500, and the gains k_a and k_b are set to 2 and 100000 respectively.

The block diagram of the test bench is shown in Fig. 4. A Chroma programmable DC power supply is used to provide 150V DC Bus voltage. The PMSM is driven by a self-made inverter, consisting of Mitsubishi intelligent power module (IPM), current and voltage hall sensors, filtering and protection

TABLE I
SPECIFICATION OF THE PMSM

Symbol	Quantity
Rated power P_N	0.75 (kW)
Rated voltage U_N	220 (V)
Rated speed n_N	3000 (rpm)
Rated torque T_N	2.4 (N·m)
Stator resistance R	1.1 (Ω)
D axis inductance L_d	8.0 (mH)
Q axis inductance L_q	8.0 (mH)
Number of pole-pairs p_n	4
Torque constant K_t	0.553 (N·m/A)
Motor inertia J	1.62×10^{-4} (kg·m^2)
Viscous friction coefficient B	5×10^{-4} (N·m·s/rad)
Coulomb friction T_c	0.1 (N·m)

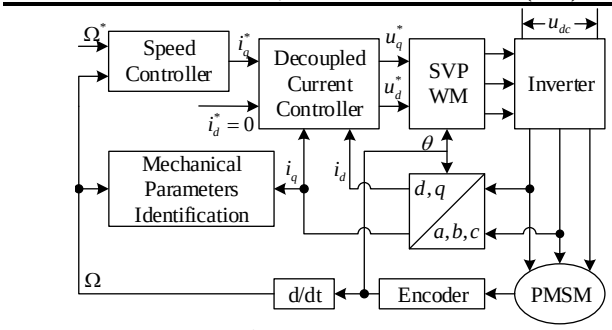

Fig. 3. The block diagram of the control system.

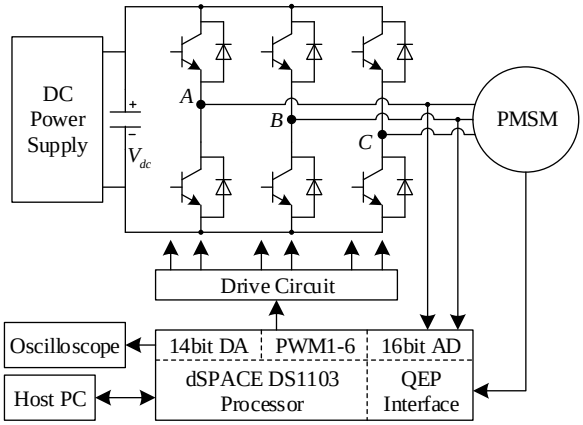

Fig. 4. The block diagram of the test bench.

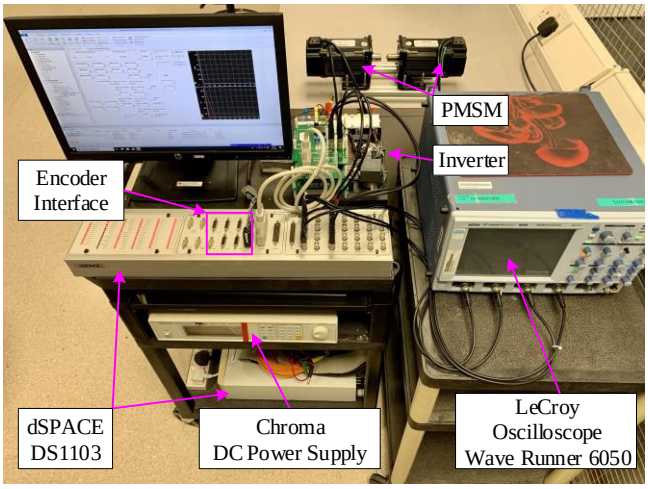

Fig. 5. Picture of the test bench.

circuit, etc. The dSPACE DS1103-based field-oriented control box is employed for driving the PMSM, as shown in Fig. 5.

To repeat the identification process, all identified parameters are reset to their initial values every 5 seconds in the experiments. The parameters of the controller in the experiment are the same as those in the simulation. The friction torque in an actual system can be measured without knowing the exact inertia, because only constant speed is needed for the measurement. The measurement results are shown in Fig. 6. To specify the Coulomb friction torque and the viscous friction coefficient from the measured friction torque values, the trend lines of the torque over speeds ranging from 50 to 2000 r/min are shown in Fig. 7.

Based on the trend lines, the Coulomb friction torque coefficient is estimated to be 0.1 N·m. The slope of the trend line from 50 to 300 r/min is 1.9×10^{-3} N·m·s/rad, and the one from 50 to 2000 r/min is 5.0×10^{-4} N·m·s/rad. Therefore, the viscous friction coefficient can be estimated in the range from 5.0×10^{-4} N·m·s/rad to 1.9×10^{-3} N·m·s/rad.

A. Effect of the LPF in Speed Feedback

In the simulation, the amplitude and the frequency of the sinusoidal speed reference are 500 r/min and 5Hz, respectively. The load torque T_L, the Coulomb friction torque coefficient T_c,

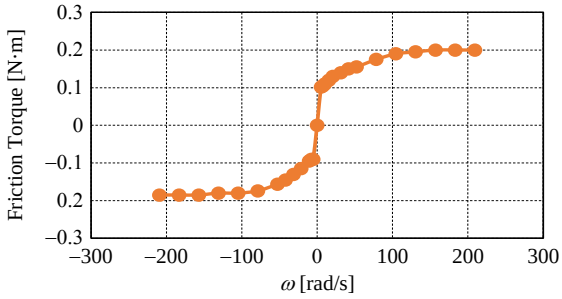

Fig. 6. Measurement of the friction torque on the servo motor.

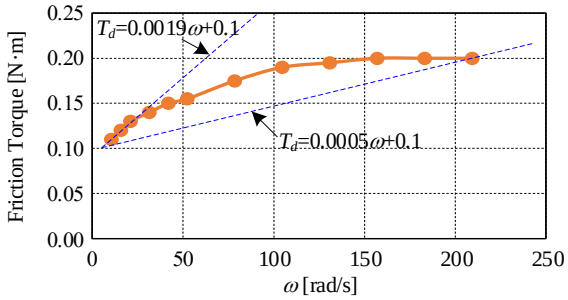

Fig. 7. Trend lines of the friction torque for a speed from 50 to 2000 r/min.

and the viscous friction coefficient B are all set to zero, and the initial estimated inertia is set to 5×10^{-5} kg·m^2. When different kinds of speeds are used as the speed feedback, the observational error, the identified moment of inertia, the identified disturbance torque, and the identified viscous friction coefficient are shown in Fig. 8.

For the cases of identification with an ideal speed without, the corresponding simulation results are shown in Fig. 8(a). The results show that the identified moment of inertia, the identified disturbance torque, and the identified viscous friction torque coefficient converges to their actual values quickly, verifying the effectiveness of the identification method.

When using the measured speed without LPF, all the identified parameters will pulsate due to the measurement noise, as shown in Fig. 8(b).

When a first order LPF with a time constant of τ=2 ms is used for filtering the measured speed, bigger pulsation is found in both the identified inertia and the identified disturbance torque before the viscous friction torque coefficient identification is enabled. However, by enabling the viscous friction coefficient identification at 3 seconds, as shown in Fig. 8(c), pulsations are eliminated. The estimated viscous friction coefficient in Fig. 8(c) converges to a negative value -3.2×10^{-4} N·m·s/rad. According to the theory, the estimated viscous friction torque coefficient is equal to $-J\tau\omega^2$, which is -3.16×10^{-4} N·m·s/rad when τ=2 ms. The simulation results are identical to the theoretical ones, which verifies the interpretation by (28).

B. Accurate Identification of the Viscous Friction Torque Coefficient

In order to identify the real viscous friction torque coefficient, the same LPF is used for the electromagnetic torque T_e. According to the theoretical analysis, before the LPF for T_e is enabled, the identified viscous friction torque coefficient

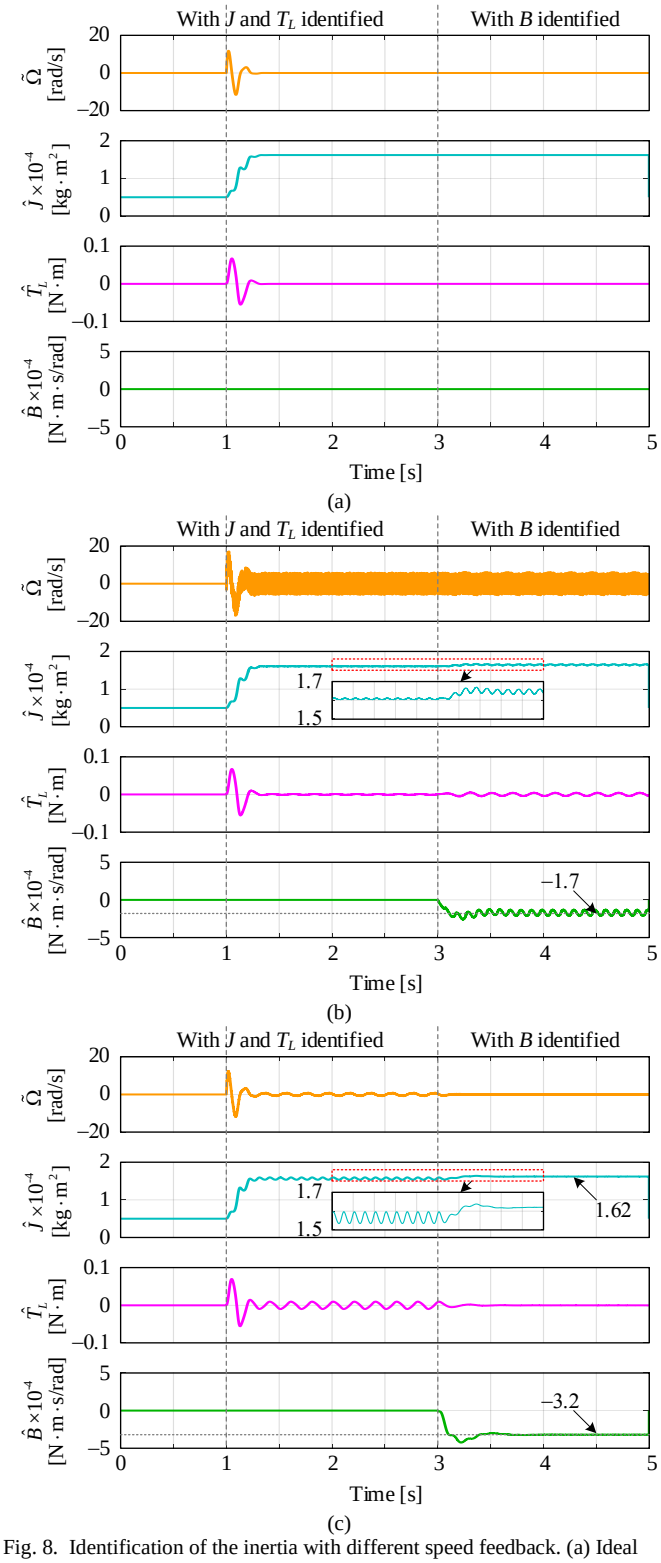

Fig. 8. Identification of the inertia with different speed feedback. (a) Ideal speed without measurement noise. (b) Measured speed without LPF. (c) Measured speed with LPF τ=2 ms.

converges to B–$J\tau\omega^2$. In Fig. 9(a) and Fig. 9(b), B=0 N·m·s/rad, the identified viscous friction torque coefficient is -1.6×10^{-4} N·m·s/rad when τ=1 ms and -3.2×10^{-4} N·m·s/rad when τ=2 ms. In Fig. 9(c), τ=1 ms and B=3×10^{-4} N·m·s/rad, the identified viscous friction torque coefficient is 1.4×10^{-4} N·m·s/rad.

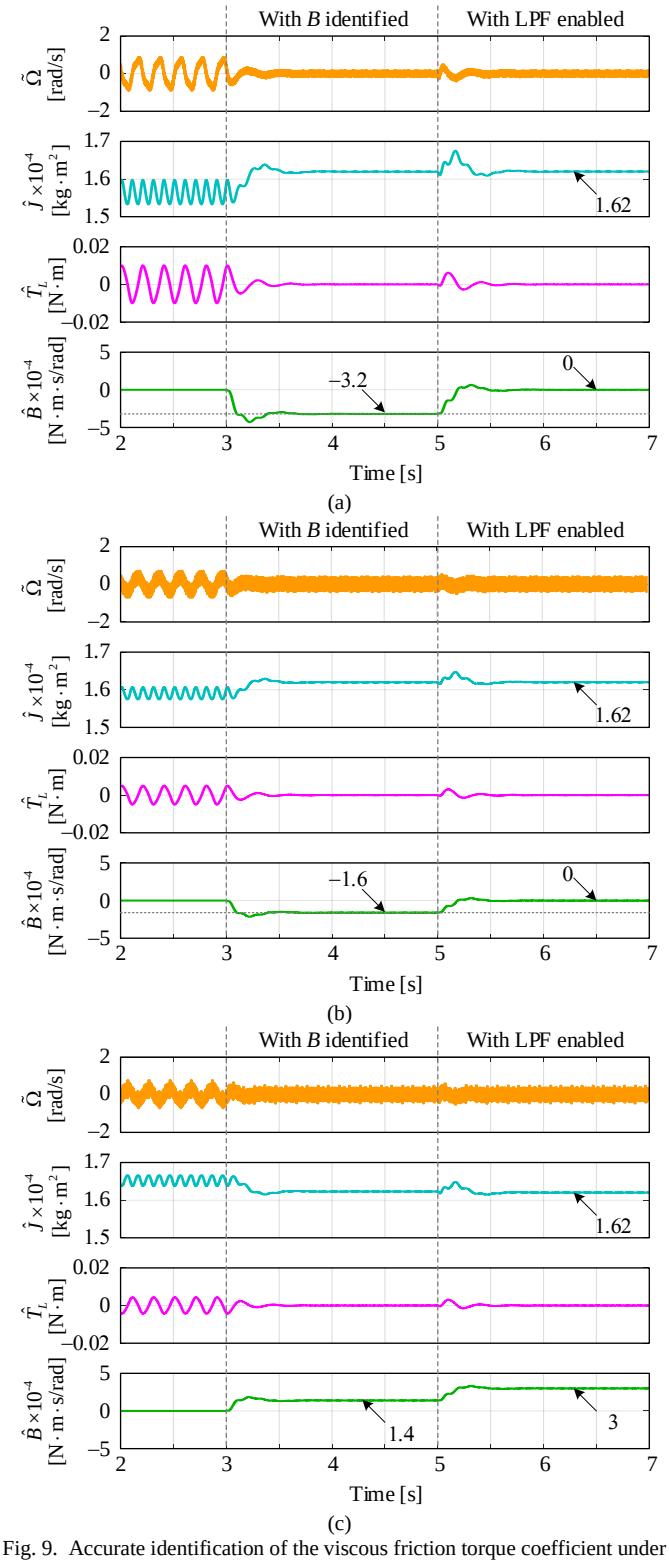

Fig. 9. Accurate identification of the viscous friction torque coefficient under different conditions. (a) τ=2 ms, B=0 N·m·s/rad. (b) τ=1 ms, B=0 N·m·s/rad. (c) τ=1 ms, B=3×10^{-4} N·m·s/rad.

Simulation results validate the method.

The strategy that using the same LPF for the speed feedback and the electromagnetic torque are verified by the above results. As a result, the strategy will be used in all the following simulations and experiments.

C. Mechanical Parameters Identification Considering the Coulomb Friction Torque.

In the simulations, the Coulomb friction torque coefficient T_c and the viscous friction torque coefficient B are set to be 0.1 N·m and 0.5×10^{-3} N·m·s/rad, respectively. The LPF with a time constant of 1 ms is adopted in both the simulations and experiments. The Coulomb friction torque is equivalent to the load torque when the motor is running in a single direction. To identify The Coulomb friction torque coefficient, the load torque should be zero, which is realistic in many applications.

Firstly, no offset is set in the sinusoidal speed reference, the corresponding simulation and experimental results are shown in Fig. 10. The simulation results show that all the identified parameters are pulsating even if the viscous friction torque coefficient identification is enabled. The identified moment of inertia converges to an error value 2.3×10^{-4} kg·m^2, and the identified viscous friction torque coefficient converges to 6.2×10^{-3} N·m·s/rad, which is much larger than its actual value.

In the experiments, the identification is repeated every 5 seconds. The identification time ranges from 0.5s to 4.5s, after that, all the identified parameters will be reset to their initial values. It can be seen from Fig. 10(b) that the identified moment of inertia also converges to the an error value 2.3×10^{-4} kg·m^2. However, due to the effect of vibration lubrication, the effective Coulomb friction torque is less than 0.1 N·m, thus the identified viscous friction torque coefficient is not so high.

Fig. 11 shows the results when the motor is running in one direction with an offset of 800 r/min. From the simulation results, it can be seen that all the identified parameters converge to their actual values without pulsation after the viscous friction torque coefficient is identified. In the experiments, the identified parameters also converge to their actual values. Nevertheless, due to the nonlinear variation of the friction torque as shown in Fig. 7, the observational error cannot be eliminated after the viscous friction torque coefficient is identified. As a result, there are still small pulsations in the steady-state identified parameters. Because the initial inertia is small, the speed tracking error is large, and the offset in the speed response is only about 400 r/min, as a result, the identified viscous friction torque coefficient converges to a bigger value, which is close to the top limit 1.9×10^{-3} N·m·s/rad.

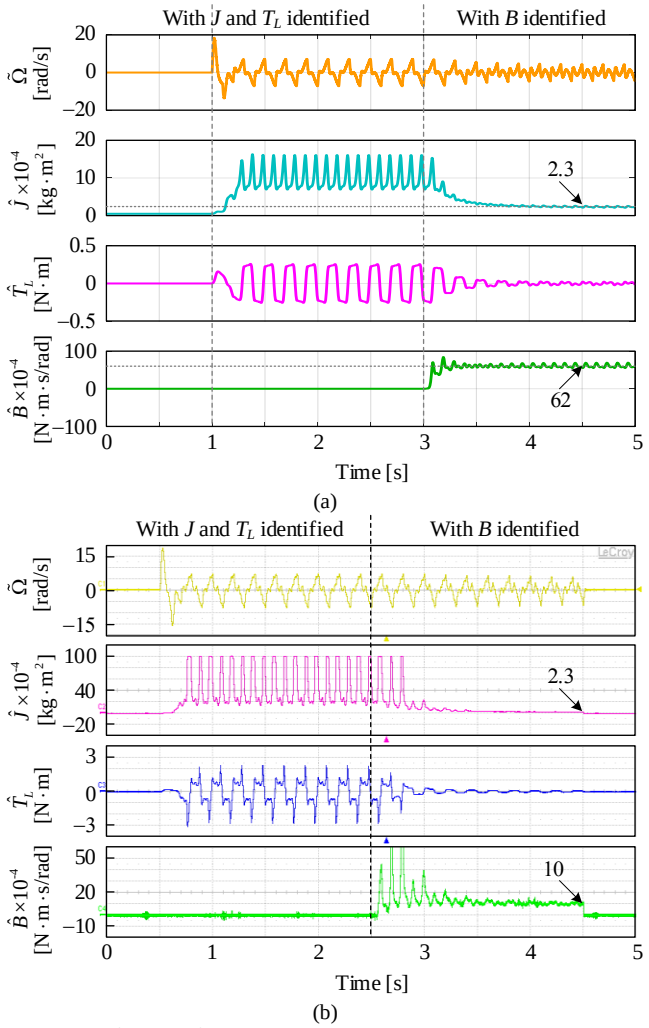

Fig. 10. Identification of the mechanical parameters under sinusoidal speed reference 500sin(10πt) r/min. (a) Simulation. (b) Experiment.

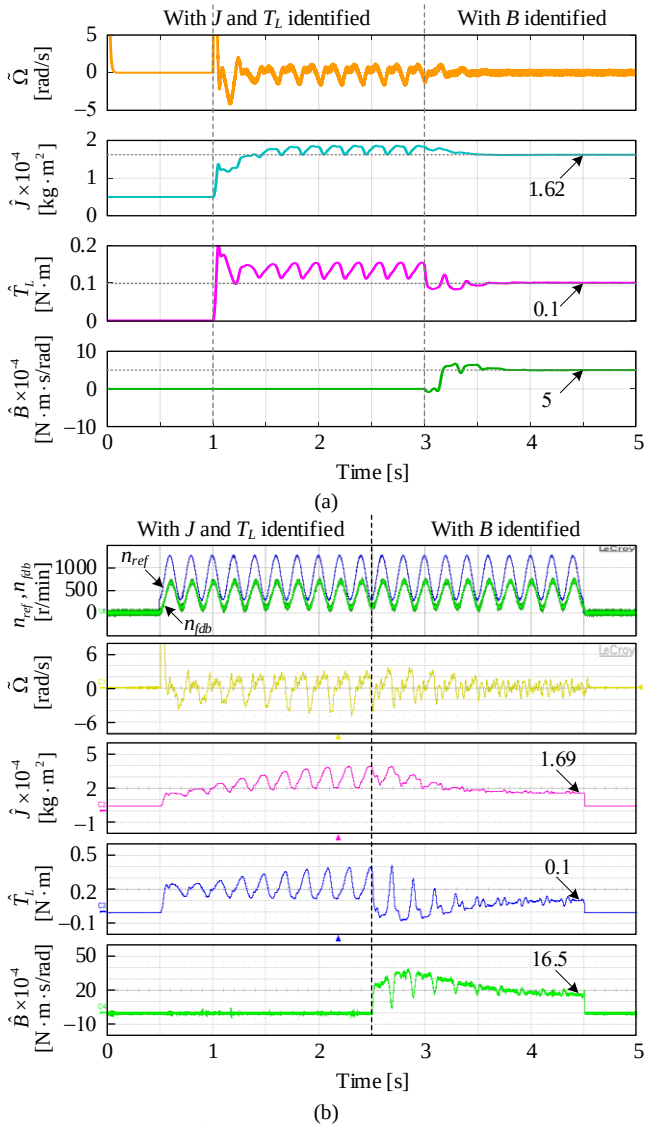

Fig. 11. Identification of the mechanical parameters under sinusoidal speed reference 500sin(10πt)+800 r/min. (a) Simulation. (b) Experiment.

When the initial inertia is changed to be 8×10^{-4} kg·m^2, which is nearly 5 times of its actual value, the identification results are shown in Fig. 12. It shows that the dynamics of the identification has been highly improved, and due to the larger offset in the speed response, the identified viscous friction torque coefficient is reduced to 9.3×10^{-4} N·m·s/rad.

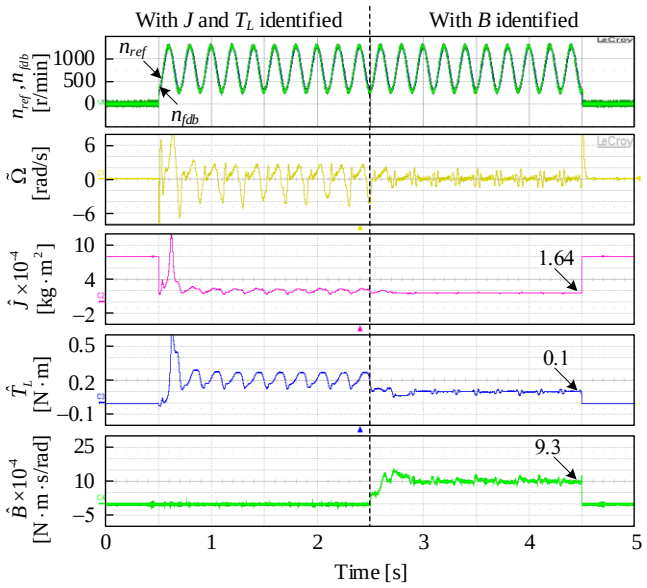

Fig. 12. Identification with an initial inertia of 8×10^{-4} kg·m^2.

Keeps the initial inertia at 8×10^{-4} kg·m^2. Reduce the gains k_a and k_b to one-fifth of their original value, i.e., k_a=0.4 and k_b=20000. The results when the speed at frequencies of 5Hz and 10Hz are shown in Fig. 13(a) and Fig. 13(b), respectively. Comparing Fig. 13(a) with Fig. 12 shows that the oscillation in the parameter identification response is reduced due to the smaller gains, but the response is slightly slower. However, the response can be improved by increasing the frequency of the speed reference, as shown in Fig. 13(b).

Keeping the initial inertia and the gains k_a and k_b, and increasing the speed offset to 1200 r/min, the identification results when the amplitude of the speed reference is 500 r/min and 250 r/min are shown in Fig. 14(a) and Fig. 14(b), respectively. It can be seen that smaller amplitude is good for reducing the pulsations before the identification of viscous friction torque coefficient, but it deteriorates the dynamics of the identification due to the smaller electromagnetic torque. Because of the larger offset, the identified viscous friction coefficient is becoming smaller, and the identified Coulomb friction torque coefficient is becoming larger.

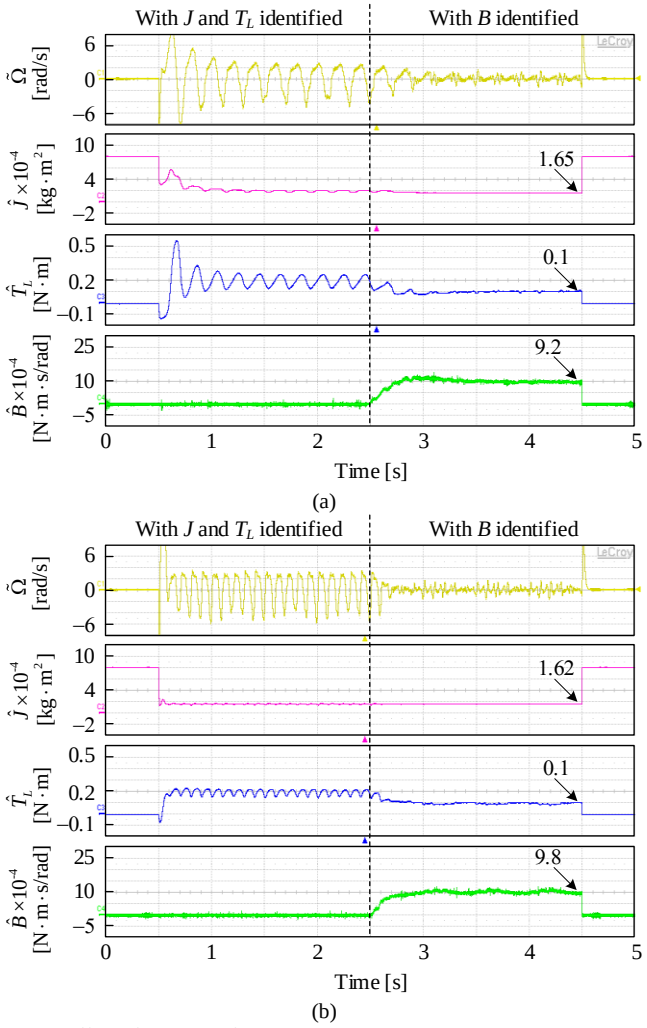

Fig. 13. Effect of the speed frequency. (a) 5Hz. (b) 10Hz.

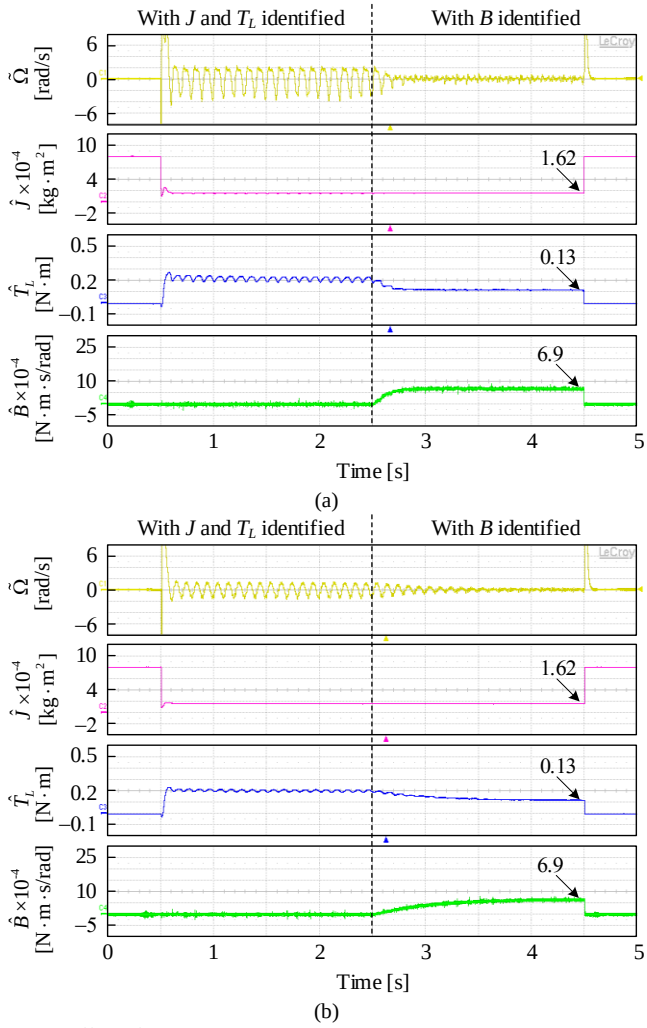

Fig. 14. Effect of the speed amplitude. (a) 500 r/min. (b) 250 r/min.

V. CONCLUSION

The contribution of this paper is to propose a method that can identify the three mechanical parameters simultaneously using only one speed. The effectiveness of the method is verified by both the simulation and experimental results.

A low pass filter is used to suppress the measurement noise in the speed feedback, thus parameters are identified with high precision. Due to the LPF used for suppressing the measurement noise in speed feedback, additional time-varying disturbance torque will be generated, resulting in a pulsating identification result. The same LPF should be used for both the speed feedback and the electromagnetic torque to eliminate the disturbance torque.

A unidirectional sine-wave speed is used to decouple the viscous friction torque and the Coulomb friction torque, two speeds with different amplitudes and the detection of the speed amplitude are no more required.

Adaptive ESO is designed based on Lyapunov's stability theory, can be easily changed to the normal ESO used for active disturbance rejection control system.

Because of the nonlinearity of the friction torque, the viscous friction coefficient is not constant over the entire speed range. The model for the servo motor mechanical system should be modified in the future. Fractional-order model may be more realistic.

REFERENCES

[1] J. Yang, W. Chen, S. Li, L. Guo, and Y. Yan, "Disturbance/Uncertainty Estimation and Attenuation Techniques in PMSM Drives—A Survey," *IEEE Trans. Ind. Electron.*, vol. 64, no. 4, pp. 3273-3285, Apr. 2017.

[2] L. Harnefors, S. E. Saarakkala and M. Hinkkanen, Speed control of electrical drives using classical control methods, *IEEE Trans. on Ind. Applicat.*, vol. 49, no.2, pp. 889-898, Mar./Apr. 2013.

[3] W. Chen, J. Yang, L. Guo, and S. Li, "Disturbance-Observer-Based Control and Related Methods—An Overview," *IEEE Trans. Ind. Electron.*, vol. 63, no. 2, pp. 1083-1095, Feb. 2016.

[4] E. Sariyildiz, R. Oboe and K. Ohnishi, "Disturbance Observer-Based Robust Control and Its Applications: 35th Anniversary Overview," *IEEE Trans. Ind. Electron.*, vol. 67, no. 3, pp. 2042-2053, Mar. 2020.

[5] J. Han, "From PID to Active Disturbance Rejection Control," *IEEE Trans. Ind. Electron.*, vol. 56, no. 3, pp. 900-906, Mar. 2009.

[6] M. Iwasaki and N. Matusi, "Robust speed control of IM with torque feedforward control," *IEEE Trans. Ind. Electron.*, vol. 40, no. 6, pp. 553-560, Dec. 1993.

[7] S. Li and Z. Liu, "Adaptive Speed Control for Permanent-Magnet Synchronous Motor System With Variations of Load Inertia," *IEEE Trans. Ind. Electron.*, vol. 56, no. 8, pp. 3050-3059, Aug. 2009.

[8] L. Niu, D. Xu, M. Yang, X. Gui, and Z. Liu, "On-line Inertia Identification Algorithm for PI Parameters Optimization in Speed Loop," *IEEE Trans. Power Electron.*, vol. 30, no. 2, pp. 849-859, Feb. 2015.

[9] Y. Zuo, X. Zhu, L. Quan, C. Zhang, Y. Du and Z. Xiang, "Active Disturbance Rejection Controller for Speed Control of Electrical Drives Using Phase-Locking Loop Observer," *IEEE Trans. Ind. Electron.*, vol. 66, no. 3, pp. 1748-1759, Mar. 2019.

[10] R. Babau, I. Boldea, T. J. E. Miller, and N. Muntean, "Complete Parameter Identification of Large Induction Machines From No-Load Acceleration–Deceleration Tests," *IEEE Trans. Ind. Electron.*, vol. 54, no. 4, pp. 1962-1972, Aug. 2007.

[11] Y. Feng, X. Yu and F. Han, "High-Order Terminal Sliding-Mode Observer for Parameter Estimation of a Permanent-Magnet Synchronous Motor," *IEEE Trans. Ind. Electron.*, vol. 60, no. 10, pp. 4272-4280, Oct. 2013.

[12] Z. Liu, H. Wei, X. Li, K. Liu, and Q. Zhong, "Global Identification of Electrical and Mechanical Parameters in PMSM Drive Based on Dynamic Self-Learning PSO," *IEEE Trans. Power Electron.*, vol. 33, no. 12, pp. 10858-10871, Dec. 2018.

[13] C. Lian, F. Xiao, S. Gao, and J. Liu, "Load Torque and Moment of Inertia Identification for Permanent Magnet Synchronous Motor Drives Based on Sliding Mode Observer," *IEEE Trans. Power Electron.*, vol. 34, no. 6, pp. 5675-5683, Jun. 2019.

[14] K. Liu, C. Hou and W. Hua, "A Novel Inertia Identification Method and Its Application in PI Controllers of PMSM Drives," *IEEE Access*, vol. 7, pp. 13445-13454, Jan. 2019.

[15] R. Garrido and A. Concha, "Inertia and Friction Estimation of a Velocity-Controlled Servo Using Position Measurements," *IEEE Trans. Ind. Electron.*, vol. 61, no. 9, pp. 4759-4770, Sep. 2014.

[16] S. Yang and K. Lin, "Automatic Control Loop Tuning for Permanent-Magnet AC Servo Motor Drives," *IEEE Trans. Ind. Electron.*, vol. 63, no. 3, pp. 1499-1506, Mar. 2016.

[17] K. Liu and Z. Zhu, "Fast Determination of Moment of Inertia of Permanent Magnet Synchronous Machine Drives for Design of Speed Loop Regulator," *IEEE Trans. Control Syst. Technol.*, vol. 25, no. 5, pp. 1816-1824, Sep. 2017.

[18] T. Kweon and D. Hyun, "High-performance speed control of electric machine using low-precision shaft encoder," *IEEE Trans. Power Electron.*, vol. 14, no. 5, pp. 838 - 849, Sep. 1999.

[19] K. Fujita and K. Sado, "Instantaneous speed detection with parameter identification for AC servo systems," *IEEE Trans. on Ind. Applicat.*, vol. 28, no. 4, pp. 864 - 872, Jul/Aug. 1992.

[20] J. W. Choi, S. C. Lee and H. G. Kim, "Inertia identification algorithm for high-performance speed control of electric motors," *in IEE Proceedings - Electric Power Applications*, vol. 153, no. 3, pp. 379-386, 1 May 2006.

[21] I. Awaya, Y. Kato, I. Miyake and M. Ito, "New motion control with inertia identification function using disturbance observer," *Proceedings of the 1992 International Conference on Industrial Electronics, Control, Instrumentation, and Automation*, San Diego, CA, USA, 1992, pp. 77-81 vol.1.

[22] F. Andoh, "Moment of Inertia Identification Using the Time Average of the Product of Torque Reference Input and Motor Position," *IEEE Trans. Power Electron.*, vol. 22, no. 6, pp. 2534-2542, Nov. 2007.

[23] Y. Chen, M. Yang, J. Long, W. Qu, D. Xu, and F. Blaabjerg, "A Moderate Online Servo Controller Parameter Self-Tuning Method via Variable-Period Inertia Identification," *IEEE Trans. Power Electron.*, vol. 34, no. 12, pp. 12165-12180, Apr. 2019.

[24] T. Kwon, S. Sul, H. Nakamura and K. Tsuruta, "Identification of the Mechanical Parameters for Servo Drive," *Conference Record of the 2006 IEEE Industry Applications Conference Forty-First IAS Annual Meeting*, Tampa, FL, 2006, pp. 905-910.

[25] S. Kim, "Moment of Inertia and Friction Torque Coefficient Identification in a Servo Drive System," *IEEE Trans. Ind. Electron.*, vol. 66, no. 1, pp. 60-70, Jan. 2019.

[26] S. W. Wang and S. M. Wan, "Estimation of load parameters for PMSM by MRAS," *in Proc. IEEE Int. Conf. Electr. Control Eng.*, 2011, pp. 657–660.

[27] K. Liu and Z. Q. Zhu, "Mechanical Parameter Estimation of Permanent-Magnet Synchronous Machines With Aiding From Estimation of Rotor PM Flux Linkage," *IEEE Trans. on Ind. Applicat.*, vol. 51, no. 4, pp. 3115-3125, Jul/Aug. 2015.

[28] A. Zaafouri, C. B. Regaya, H. B. Azza, and A. Châari, "DSP-based adaptive backstepping using the tracking errors for high-performance sensorless speed control of induction motor drive," *ISA Transactions*, 2015.

[29] C. B. Regaya, F. Farhani, A. Zaafouri, and A. Chaari, "An adaptive sliding-mode speed observer for induction motor under backstepping control," Innovative Computing, Information and Control, vol 11, no. 4, pp.763-771, Apr. 2017.

Yuefei Zuo (M'18) received the B.Sc. and the Ph. D. degrees in electrical engineering and automation from Nanjing University of Aeronautics and Astronautics, Nanjing, China, in 2010 and 2016, respectively.

He has been working as a Lecturer at Jiangsu University since July 2016. He is currently a Postdoctoral Research Fellow with the School of Electrical and Electronic Engineering, Nanyang Technological University, Singapore. His research interests include advanced control strategies for high performance electric drives.

Jie Mei (S'13) received his B.S. degree in electrical engineering from the School of Electrical and Computer Engineering, Georgia Institute of Technology, Atlanta, GA, USA, in 2015. He is currently pursuing his Ph.D. degree at the Department of Electrical Engineering and Computer Science, Massachusetts Institute of Technology, Cambridge, MA, USA. His research interests include Electric Machines, Multi-Carrier Energy System, and Electric Vehicle Technologies.

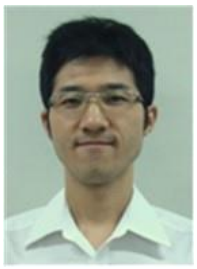

Xinan Zhang (S'10, M'14) received the B.E. degree in electrical engineering and automation from Fudan University, China, in 2008. He received the Ph.D. degree from Nanyang Technological University (NTU), Singapore, in 2014. Then, he worked as postdoc researcher in NTU and the University of New South Wales from 2014 to 2017. He worked as a Lecturer in NTU from June 2017 to September 2019. Since September 2019, he joined the University of Western Australia as a Senior Lecturer. His research interests include electrical machine drives, control and modulation of power electronic converters and management of hybrid energy storage systems.

Christopher H. T. Lee (M'12-SM'18) received his B.Eng. (First Class Honours) degree, and Ph.D. degree both in electrical engineering from Department of Electrical and Electronic Engineering, The University of Hong Kong, Hong Kong.

He currently serves as an Assistant Professor at Nanyang Technological University, Singapore, a Visiting Assistant Professor at Massachusetts Institute of Technology, United States, and also a Honorary Assistant Professor at The University of Hong Kong, Hong Kong. He is an Associate Editor for IEEE Access and IET Renewable Power Generation. His research interests include Electric Machines and Drives, Renewable Energies, and Electromechanical Propulsion Technologies. In these areas, he has published 1 book, 3 books chapters, and over 80 referred papers.

Dr. Lee has received many awards, including NRF Fellowship, Nanyang Assistant Professorship, Li Ka Shing Prize (the best Ph.D. thesis prize) and Croucher Foundation Fellowship.